ELSEVIER

S0011-2275(96)00046-X

Cryogenics **36** (1996) 829–841

0011-2275/96/$15.00

Sloshing of cryogenic helium driven by lateral impulse/gravity gradient-dominated/or *g*-jitter-dominated accelerations and orbital dynamics

R.J. Hung, Y.T. Long and G.J. Zu

The University of Alabama in Huntsville, Huntsville, AL 35899, USA

The coupling of slosh dynamics within a partially filled rotating dewar of superfluid helium II with spacecraft orbital dynamics is investigated in response to the environmental disturbances of (a) lateral impulses, (b) gravity gradients and (c) *g*-jitter forces. The purpose of this study is to investigate how the coupling of helium II fluid slosh dynamics driven by three cases of environmental force with spacecraft dynamics can affect the bubble deformations and their associated fluid and spacecraft mass centre fluctuations. The numerical computation of slosh dynamics is based on a rotational frame, while the spacecraft dynamics is associated with a non-rotational frame. Results show that the major contribution of orbital dynamics is driven by coupling with slosh dynamics. Neglecting the effect of slosh dynamics acting on the spacecraft may lead to the wrong results for the development of orbital and attitude control techniques.

Keywords: He II, slosh dynamics; lateral impulse; gravity gradient force; *g*-jitter force; spacecraft dynamics; microgravity

In order to carry out scientific experiments, some experimental spacecraft use cryogenic cooling for telescope instrumentation, and occasionally to maintain temperatures near absolute zero for mechanical stability. Most frequently, the cryogen used is helium II. In this study, the coupling of spacecraft orbital dynamics with sloshing of helium II driven by lateral impulses, gravity gradients and *g*-jitter forces is investigated. Both gravity gradients and *g*-jitter forces will be defined later. In the specific case of the Gravity Probe-B (GP-B), the spacecraft uses liquid helium as a cryogen and propellant to maintain the cooling of instruments, attitude control and drag-free operation of the spacecraft. Potential fluid management problems may arise due to an asymmetric distribution of liquid helium and helium vapour due to perturbations in the liquid–vapour interface. A basic understanding of the coupling of slosh dynamics in six degrees of freedom with orbital dynamics plays a significant role in the development of spacecraft guidance and attitude control systems.

Liquid helium at a temperature of 1.8 K is used on the GP-B. Because it is a superfluid, there are at most only very small temperature gradients in the liquid helium. In the absence of Marangoni convection, due to the negligibly small temperature dependence of surface tension and negligible thermal gradients along the liquid–vapour interface, the equilibrium shape of the interface is governed by a balance of capillary, centrifugal, gravitational and dynamic forces. Determination of liquid–vapour interface profiles based on computational experiments can uncover details of the flow that cannot be easily visualized or measured experimentally in a microgravity environment.

An instability of the liquid–vapour interface can be induced by the presence of longitudinal and lateral accelerations. Thus, slosh waves are excited, producing high- and low-frequency oscillations in the liquid helium. The sources of the residual accelerations include effects of the Earth's gravity gradient and *g*-jitter[1–3]. A recent study[4] suggests that the high-frequency accelerations may be unimportant in comparison with the residual motions caused by low-frequency accelerations.

The time-dependent behaviour of liquid helium in a partially filled rotating dewar in reduced gravity environments was simulated by numerically solving the Navier–Stokes equations subject to initial and boundary conditions[5,6]. At the interface between the liquid and vapour, both the kinematic surface boundary condition and the interface stress conditions for components tangential and normal to the interface were applied[2–3]. The initial conditions were adopted from the steady-state formulations developed by Hung *et al.*[7]. Some of the steady-state formulations of interface shapes were compared with the available experiments carried out by Leslie[8] in a free-falling aircraft (KC-135).

The experiments of Mason *et al.*[9] showed that classical fluid mechanics theory is applicable to cryogenic helium in large containers with sufficiently large velocities[10–13].

At temperatures close to absolute zero, quantum effects begin to be of importance in the properties of fluids. At a temperature of 2.17 K, liquid helium undergoes a second-order phase transition; at temperatures below this point, liquid helium (helium II) has a number of remarkable properties, the most important of which is superfluidity. This is the property of being able to flow without viscosity in narrow capillaries or gaps. At temperatures other than zero, helium II behaves as if it were a mixture of two different liquids. One of these is a superfluid and moves with zero viscosity along a solid surface. The other is a normal viscous fluid. The two motions occur without any transfer of momentum from one to the other for velocities below a critical velocity[10–12]. Above the critical velocity, the two fluids are coupled through their mutual friction[10–15].

The key parameters affecting critical velocity are temperature and container size. To determine the dynamic behaviour of helium II in a large rotating cylinder, the mutual friction of the two fluid components is accounted for in the model computation. The density concentration of the superfluid is a function of temperature, which is also true for the surface tension and viscous coefficient for helium II[10–17]. In this study, the theory of viscous Newtonian fluids is employed with transport coefficients being a function of temperature.

In order to carry out the study of transient phenomena of coupling between slosh reaction torques driven by three types of acceleration and spacecraft orbital dynamics, (a) slosh dynamics based on a fluid dynamics formulation and (b) orbital dynamics based on translational and rotational formulations of spacecraft dynamics, have been numerically solved simultaneously. The three types are (a) lateral impulse, (b) gravity gradient-dominated and/or (c) g-jitter-dominated accelerations. In other words, coupling between slosh dynamics and orbital dynamics will deeply affect the behaviour of the bubble driven by slosh dynamics, which is quite different from the results obtained earlier[15,18] without the implementation of the orbital dynamics modification. Meanwhile, it is true that orbital dynamics driven by slosh dynamics can cause the spacecraft to deviate from normal operation[19].

Non-inertial frame mathematical formulation of slosh dynamics

An experiment by Andronikashvili[10–13] for rotating helium II showed that it is necessary to exceed a critical velocity for the interaction between the normal and superfluid components to establish rotation of the entire bucket[10–13]. For a rotating dewar with outer diameter 1.56 m and inner diameter 0.276 m, the critical velocities are 6.4×10^{-7} and 3.6×10^{-6} m s^{-1}, respectively[10–15]. With a rotating speed of 0.1 rev min^{-1}, the linear velocities along the outer and inner walls of a rotating dewar are 8.17×10^{-3} and 1.45×10^{-3} m s^{-1}, respectively, which are at least several hundred times greater than the corresponding critical velocities. Based on this illustration, the problem under consideration has the necessary features for a viscous Newtonian fluid formulation to be adopted in this study.

Consider a closed circular dewar partially filled with helium II. The whole fluid system is spinning in the axial direction z of cylindrical coordinates (r, θ, z), with corresponding velocity components (u, v, w). The governing equations for non-inertial frame bound coordinates of a spacecraft spinning along its z-axis have been given in recent studies[20–22]. Thus, dynamic forces relating to gravity gradient, g-jitter and angular accelerations, and centrifugal, Coriolis, surface tension, viscous forces, etc., are given explicitly in the mathematical formulations[18 22]. In the computation of sloshing reaction forces, moments, viscous stress and angular momentum acting on the container wall of the spacecraft, one must consider those forces and moments in the inertial frame rather than in the non-inertial frame[20 24].

For the purpose of solving slosh dynamic problems of liquid systems in orbital spacecraft under a microgravity environment, one must solve the governing equations[21,23] accompanied by a set of initial and boundary conditions. A precise and detailed illustration of these initial and boundary conditions was given by Hung and Pan[19–22,24]. The computational algorithm applicable to cryogenic fluid management under microgravity was also given earlier[20–24]. Summarized computational algorithms are illustrated in *Figure 1*. In this study, in order to show a realistic example, a dewar with an outer radius of 0.78 m, and an inner radius of 0.138 m, top and bottom radii of 1.10 m and a height of 1.62 m has been used in the numerical simulation. The

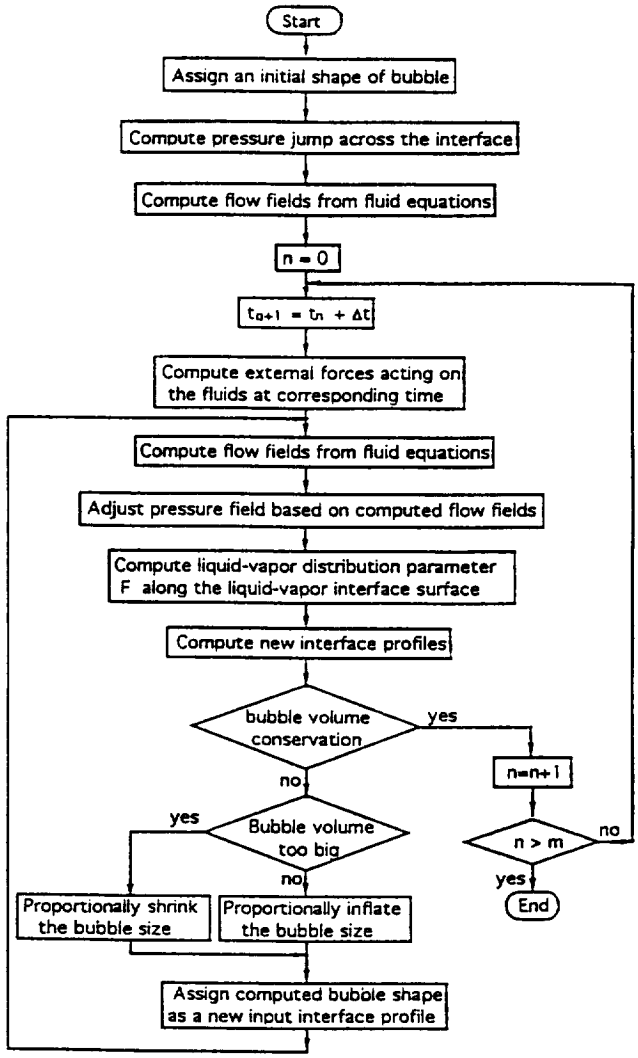

Figure 1 Computational algorithm for slosh dynamics

dewar tank is 80% filled with liquid helium and the ullage is filled with helium vapour (total fluid mass 287.6 kg). The temperature of liquid helium is 1.8 K. In this study the following data were used: liquid helium density = 145.7 kg m^{-3}, helium vapour density = 0.45 kg m^{-3}, fluid pressure = 1.6625 Pa, surface tension coefficient at the interface between liquid helium and helium vapour = 0.0353 N m^{-1}, liquid helium viscosity coefficient = 9.61×10^{-9} m^2 s^{-1} and contact angle = 0°. The initial profiles of the liquid–vapour interface for the rotating dewar are determined from computations based on algorithms developed for the steady-state formulation of microgravity fluid management[7,25].

A staggered grid for the velocity components is used in this computer program. The MAC (marker-and-cell) method[26] of studying fluid flows along a free surface is adopted and the VOF (volume of fluid) method is used to solve finite difference equations numerically. The approximate flow velocity is calculated from the explicit approximation of momentum equations based on the results from the previous time step. Computation of pressure and velocity at the new time step are thus obtained from iteratively solving the pressure equation through the conjugate residual technique[27–30]. The configuration of the liquid–vapour interface adjusted by the surface tension effect at the new time step is then obtained. The time step during this computation is automatically adjusted through the fulfilment of the stability criteria of computed grid size. The convergence criterion of the iteration of the pressure equation is based on the computed velocity at each cell which satisfies the continuity equation with errors of no more than 10^{-5} in the velocity difference[31]. As for the volume conservation of liquid, a deviation of less than 1% error in volume is guaranteed before moving to the next time step.

In this study, characteristics of the slosh reaction forces and torque fluctuations exerted on the dewar in response to various accelerations acting on the spacecraft are also investigated. The mathematical formulation of the fluctuations of slosh reaction forces and torques exerted on the dewar are illustrated elsewhere[21,32,33]. With reference to slosh dynamics driven by impulse[15,19] and mathematical formulations[21,32,33], one can calculate the slosh reaction force and the associated torque acting on the dewar, calculations that are required for the computation of the coupling of the slosh dynamics of He II with the orbital dynamics illustrated in the next section.

Inertial frame mathematical formulation of spacecraft dynamics

In spacecraft dynamics, a rigid body with six degrees of freedom, three being translational and three rotational, is considered. In this study, our primary interest is to investigate the coupling between slosh reaction torques driven by (a) lateral impulse, (b) gravity gradient-dominated and (c) *g*-jitter-dominated accelerations and spacecraft dynamics. In other words, our main purpose of study is to investigate how the coupling of slosh reaction forces/torques with spacecraft dynamics can affect cryogenic bubble deformations and their associated fluid and spacecraft mass centre fluctuations.

The three governing translational equations are given by

$$\frac{d}{dt}(m\dot{X}_i) = F_{Di} + F_{Li} \tag{1}$$

where m, X, F_D and F_L denote the mass of the spacecraft, the inertial frame (non-rotational) coordinate, the residual environmental force acting on the spacecraft and the slosh reaction force (from the fluid system) acting on the spacecraft, respectively[19,20,30,31]. Subscript i denotes components along the i-direction (= X, Y or Z in the non-rotational frame), while single and double overdots imply first- and second-order time derivatives of a parameter, respectively. Eulerian angles are defined to accommodate three rotational equations[34]. As usual, ψ, θ and ϕ are defined as the heading, attitude and bank angles[34]. Three rotational equations in terms of Eulerian angles are given by

$$I_t(\ddot{\theta} + \dot{\psi}^2 \sin\theta\cos\theta) + I_a\dot{\psi}\cos\theta(\dot{\phi} - \dot{\psi}\sin\theta) = M_\theta \tag{2}$$

$$I_a[(-\ddot{\phi} + \ddot{\psi}\sin\theta + \dot{\psi}\dot{\theta}\cos\theta)\sin\theta - \dot{\theta}(\dot{\phi} - \dot{\psi}\sin\theta)\cos\theta] + I_t(\ddot{\psi}\cos^2\theta - 2\dot{\psi}\dot{\theta}\sin\theta\cos\theta) = M_\psi \tag{3}$$

$$I_a(\ddot{\phi} - \ddot{\psi}\sin\theta - \dot{\psi}\dot{\theta}\cos\theta) = M_\phi \tag{4}$$

where

$$M_\theta = (M_{Lx} + M_{Dx})\cos\phi - (M_{Ly} + M_{Dy})\sin\phi \tag{5}$$

$$M_\psi = (M_{Lx} + M_{Dx})\sin\phi\cos\theta + (M_{Ly} + M_{Dy})\cos\phi\cos\theta - (M_{Lz} + M_{Dz})\sin\theta \tag{6}$$

$$M_\phi = (M_{Lz} + M_{Dz}) \tag{7}$$

Here M_{Li} and M_{Di} are the slosh reaction torque acting on the dewar and the residual torque acting on the spacecraft, respectively, along the i-direction (i= x, y or z in the non-inertial frame). I_a (= I_{zz}) and I_t (= I_{xx} = I_{yy}) denote the moments of inertia along the axial and transverse directions, respectively.

Activation of the coupling of slosh dynamics in response to lateral impulse and environmental disturbances, such as gravity and *g*-jitter accelerations, with spacecraft dynamics certainly will induce angular velocities (ω_1,ω_2,ω_3) along with (x,y,z) coordinates in the rotational frame. We can assume that (ω_1,ω_2,ω_3) = ($\dot{\theta}_1$,$\dot{\theta}_2$,$\dot{\theta}_3$ + ω). Here ($\dot{\theta}_1$,$\dot{\theta}_2$,$\dot{\theta}_3$) are the time derivatives of the angular displacements along the (x,y,z) coordinates and ω denotes the rotational speed along the z-axis. With the definitions $I_{xx} = I_1$, $I_{yy} = I_2$ and $I_{zz} = I_3$, the spinning angular velocity in the rotational frame can be expressed as follows:

$$\begin{aligned}
\ddot{\theta}_1 + K_2\dot{\theta}_2(\dot{\theta}_3 + \omega) &= \frac{1}{I_1}(M_{Lx} + M_{Dx}) \\
\ddot{\theta}_2 + K_2\dot{\theta}_1(\dot{\theta}_3 + \omega) &= \frac{1}{I_2}(M_{Ly} + M_{Dy}) \\
\ddot{\theta}_3 + K_3\dot{\theta}_1\dot{\theta}_2 &= \frac{1}{I_3}(M_{Lz} + M_{Dz})
\end{aligned} \tag{8}$$

where $K_1 = (I_3 - I_2)/I_1$, $K_2 = (I_1 - I_3)/I_2$ and $K_3 = (I_2 - I_1)/I_3$.

Both the translational and rotational equations are initial-value problems. Initial conditions for the translational and rotational equations are

$$\left.\begin{aligned}(X, Y, Z) &= (0, 0, 0)\ \text{cm} \\ (\dot{X}, \dot{Y}, \dot{Z}) &= (0, 0, 0)\ \text{cm s}^{-1}\end{aligned}\right\} \quad \text{at } t = 0 \tag{9}$$

$$\left.\begin{array}{l}(\theta, \psi, \phi) = (0, 0, 0) \text{ rad} \\ (\dot{\theta}, \dot{\psi}, \dot{\phi}) = (0, 0, 0.1) \text{ rev min}^{-1}\end{array}\right\} \quad \text{at } t = 0 \qquad (10)$$

In order to solve the coupling of slosh dynamics and spacecraft orbital dynamics, as shown in Equations (1) to (4), an iteration method at every time step was adopted to determine (F_{Di}, M_{Di}) for spacecraft that are mutually coupled with (F_{Li}, M_{Li}) from the slosh dynamics. The summarized computational algorithm is illustrated in *Figure 2*, where the superscript k is the number of the iteration. In this computation, the dry mass of the spacecraft (excluding the fluid mass) is assumed to be 350 kg, the fluid mass with an 80% liquid-filled level is 287.6 kg and the moment of inertia for the spacecraft is $I_{xx} = I_{yy} = 160.3$ kg m^2, and $I_{zz} = 154.5$ kg m^2.

Coupling of He II slosh dynamics and orbital dynamics

The characteristics of the three types of force on fluid systems are quite different. The lateral impulse is in the form of a spotty δ-function with a short time period of 10^{-2} s, while both the gravity gradient and the g-jitter forces are in the form of a continuous spectrum covering the whole spacecraft orbit period. The magnitudes of these accelerations vary from 10^{-2} to 10^{-9} g_o (where $g_o = 9.81$ m s^{-2}) and act on fluid elements at different locations either with different magnitudes (gravity gradient forces) or the same magnitudes (impulse and g-jitter forces), depending on their characteristics. These are illustrated in *Table 1* with a full description shown in this section.

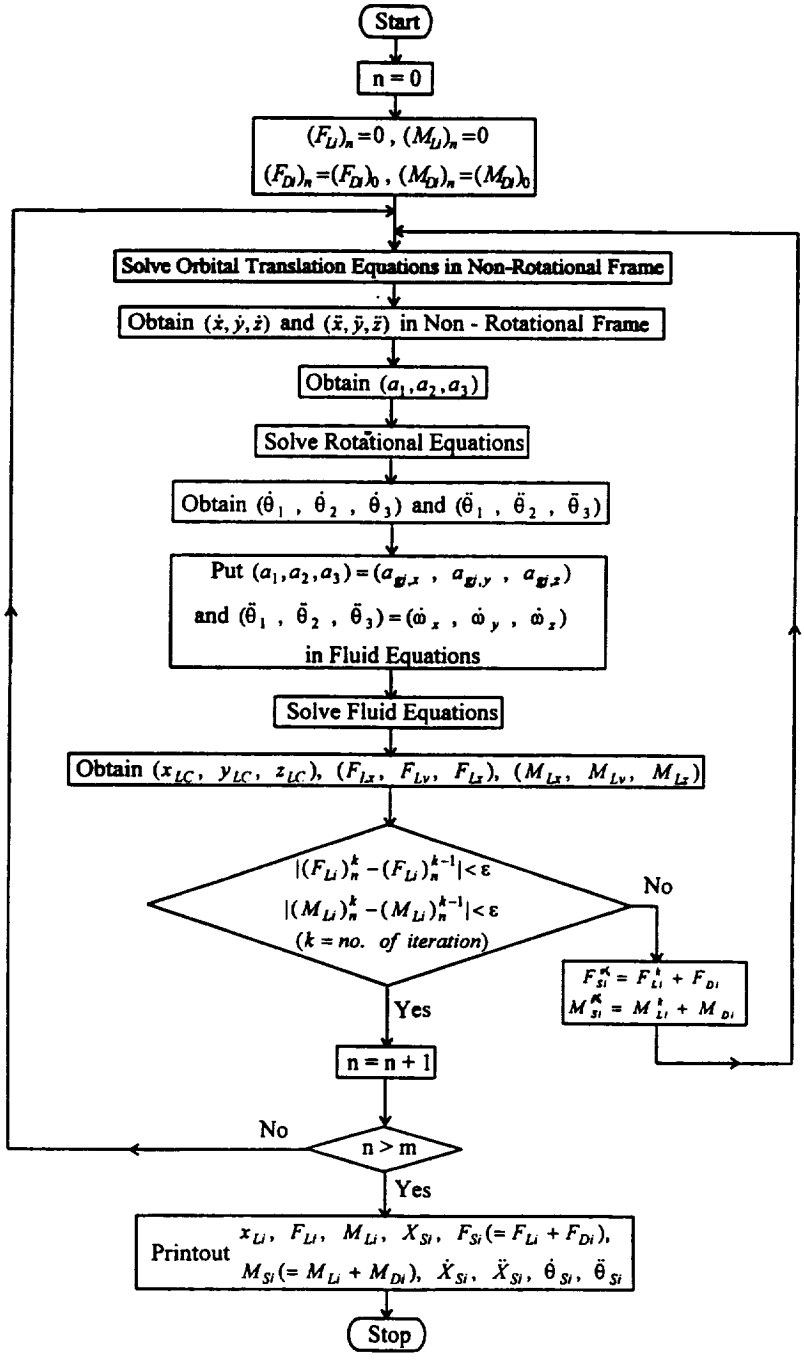

Figure 2 Computational algorithm for coupling of slosh and orbital dynamics

Table 1 Characteristics of various orbital accelerations driven slosh dynamics

	Lateral impulse	Gravity-gradient-dominated	*G*-jitter-dominated
Types of forces	Spotty δ-function	Continuous spectrum	Continuous spectrum
Magnitudes of forces	$10^{-3}\ g_o$	$10^{-7}\ g_o$	$10^{-6}\ g_o$
Time period of force acting	10^{-2} s	Full orbit period	Full orbit period
Magnitude ranges of forces	(10^{-2} to 10^{-9}) g_o	$10^{-7}\ g_o$	(10^{-5} to 10^{-9}) g_o
Magnitudes of force acting on fluid element at different locations	Same magnitude	Different magnitudes	Same magnitude
Types of fluid motions	Leftward and rightward oscillations	Tidal mode motion	Leftward–rightward and up–down oscillations
Maximum fluid mass centre fluctuations (cm)	2	1.4	5

Coupling between lateral impulse driven slosh dynamics and spacecraft dynamics

It is assumed that a lateral impulse with the following forms of force (F_i) and torque (M_i) acts on the spacecraft system in non-inertial (rotating) frame Cartesian coordinates[15,18]:

$$\left.\begin{aligned} F_i &= (F_x, F_y, F_z) = (20, 0, 0)\ \text{N} \\ M_i &= (M_x, M_y, M_z) = (0, 10, 0)\ \text{N m} \end{aligned}\right\} \quad \text{for } 0 \le t \le 10^{-2}\ \text{s} \tag{11}$$

and

$$\left.\begin{aligned} F_i &= (0, 0, 0)\ \text{N} \\ M_i &= (0, 0, 0)\ \text{N m} \end{aligned}\right\} \quad \text{for } t > 10^{-2}\ \text{s} \tag{12}$$

For a spacecraft mass of 637.6 kg, the lateral impulse is equivalent to $3.2 \times 10^{-3} g_o$ in this case. In general, the magnitude range of the lateral impulses is 10^{-2} to $10^{-9} g_o$.

The entire computation of the slosh dynamics is carried out for coupling with the spacecraft dynamics. Slosh dynamics concluded from the present study are quite different from the results obtained earlier[15,18] without the consideration of spacecraft dynamics. *Figure 3* shows the time-sequence evolution of the three-dimensional dynamic behaviour of the liquid–vapour interface (bubble) oscillations (in the rotational frame) activated by a lateral impulse acting on the spacecraft in the positive x-direction and reacting to the fluid in the negative x-direction (liquid in negative x-, and bubble in positive x-directions). The time-sequence evolution illustrates the following behaviour of the bubble dynamics in response to a lateral impulse: (a) the bubble was first shifted to the positive x-direction (liquid to the negative x-direction); (b) the bubble was also shifted to the positive y-direction due to the Coriolis force with rotation along the z-axis in the rotational frame; and (c) bubble deformations with back-and-forth oscillations are viewed during the 1500 s simulation time span.

Figure 4A shows the time evolution of the growth and decay of fluid mass centre fluctuations (in the rotational frame) in response to a lateral impulse. It is also due to the torque of the impulse acting on the y-axis which drives the propagating slosh dynamic disturbances to the z-axis. The values of the maximum and minimum locations of the fluid mass centre fluctuations are Max (x_{LC}, y_{LC}, z_{LC}) = (0.46, 10^{-4}, 0.25) cm and Min (x_{LC}, y_{LC}, z_{LC}) = (−1.3, −1.9, −0.28) cm, respectively, while the fluctuating values of the maximum fluid mass centre disturbances are Max (Δx_{LC}, Δy_{LC}, Δz_{LC}) = (1.73, 1.93, 0.53) cm. This shows that $\Delta y_{LC} > \Delta x_{LC} > \Delta z_{LC}$. The response to a lateral impulse can be described as follows: (a) the fluid mass was shifted to the negative x-direction initially due to the dewar reaction force acting on the fluid in response to the impulse on the spacecraft in the positive x-direction; (b) the shift in the fluid mass centre fluctuations to the negative y-direction in the rotational frame was also caused by the dewar reactional Coriolis force acting on the fluid in response to the impulse; (c) this shows that the major fluid mass centre fluctuations are in the negative x, negative y quadrant with small ripple oscillations in the z-axis; (d) there is a time lag of 150 s between the impulse acting on the spacecraft and the maximum fluid mass centre displacement; in other words, the fluid mass centre reacted rather slowly; (e) *Figure 4B* shows an exponential decay in the time history of the fluid mass centre fluctuations with a very long time constant because of the extremely low surface tension and viscosity of helium II fluids.

The spacecraft mass centre fluctuations (in a non-rotational frame) were also studied, as illustrated in *Figure 4C*. The maximum and minimum locations of the spacecraft mass centre fluctuations are Max (X_{sc}, Y_{sc}, Z_{sc}) = (0.85, 0.63, −0.24) cm and Min (X_{sc}, Y_{sc}, Z_{sc}) = (−0.6, −0.76, −0.50) cm, respectively, while the fluctuating values of the maximum spacecraft mass centre disturbances are Max (ΔX_{sc}, ΔY_{sc}, ΔZ_{sc}) = (1.46, 1.39, 0.26) cm. This shows that $\Delta X_{sc} > \Delta Y_{sc} > \Delta Z_{sc}$ in a non-rotational frame. The spacecraft mass centre fluctuations are very similar to those of the fluid obtained in *Figures 4A* and *4B* except that the former is in a non-rotational frame, and the latter in a rotational frame in which the Coriolis force transfers a disturbance from the X- to the Y-axis. The magnitude is smaller by the ratio of the liquid weight to the total spacecraft weight. *Figure 4D* shows the time history of the spacecraft mass centre displacement. Clearly the effects of helium slosh must be considered in the spacecraft attitude control systems.

Coupling between slosh dynamics driven by combined gravity gradient and g-jitter accelerations dominated by gravity gradient forces and spacecraft dynamics

To give an example of the GP-B spacecraft, which is an Earth satellite orbiting at 650 km directly over the poles, the orbit period, τ_o, can be computed from the following expression:

$$\tau_o = 2\pi \frac{R_c^{3/2}}{R_E g_o^{1/2}} \tag{13}$$

where R_E denotes the radius of the Earth (= 6373 km), R_c

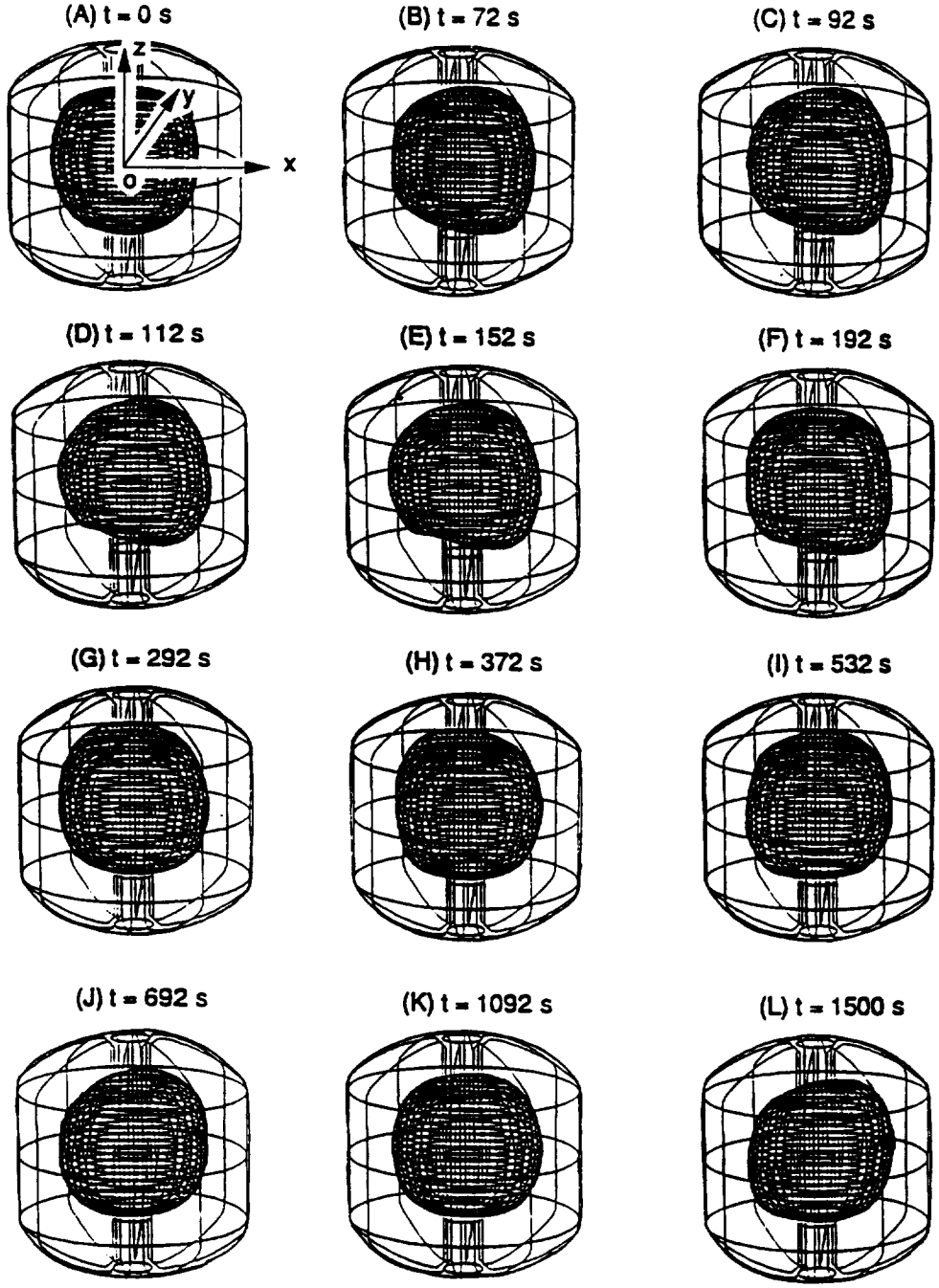

Figure 3 Three-dimensional bubble deformations in response to coupling between lateral impulse and orbital dynamics

the radius of the circular orbit ($= R_E + h = 7023$ km), h the orbit altitude ($= 650$ km) and g_o the Earth's gravity acceleration. For the case of GP-B, the orbit period $\tau_o = 97.6$ min (5856 s), and the orbit rate $n = 2\pi/\tau_o = 1.07 \times 10^{-3}$ rad s^{-1}.

The gravity gradient acceleration acting on the fluid mass of the spacecraft can be given by[18–20]

$$\hat{\mathbf{a}}_{gg} = -n^2[3(\hat{\mathbf{r}}_c \cdot \hat{\mathbf{d}})\hat{\mathbf{r}}_c - \hat{\mathbf{d}}] \quad (14)$$

where $\hat{\mathbf{a}}_{gg}$ denotes the gravity gradient acceleration vector, $\hat{\mathbf{d}}$ the vector (not a unit vector) from the fluid element to the spacecraft mass centre, $\hat{\mathbf{r}}_c$ a unit vector in the direction from the spacecraft mass centre to the centre of the Earth and n the orbit rate.

In the case of the GP-B spacecraft, it is assumed that the gravity gradient exerted on the mass centre (balanced by the centrifugal forces of the orbiting spacecraft) is zero when the spacecraft is moving around the Earth on its specified orbit. In other words, the gravity acceleration exerted on the spacecraft consists only of the gravity gradient acceleration which is defined in Equation (14). *Figure 5A* illustrates the geometrical relationship between the parameters shown in Equation (14).

At time $t = 0$, the rotating axis of the spacecraft is aligned with the radial direction from the centre of the Earth to the spacecraft mass centre. The azimuth angle of the Earth towards the location of the spacecraft mass centre, ψ_E, can be computed from the orbit period obtained from Equation (13) under normal operation of the spacecraft:

$$\psi_E = 2\frac{\pi}{\tau_o}t \quad (15)$$

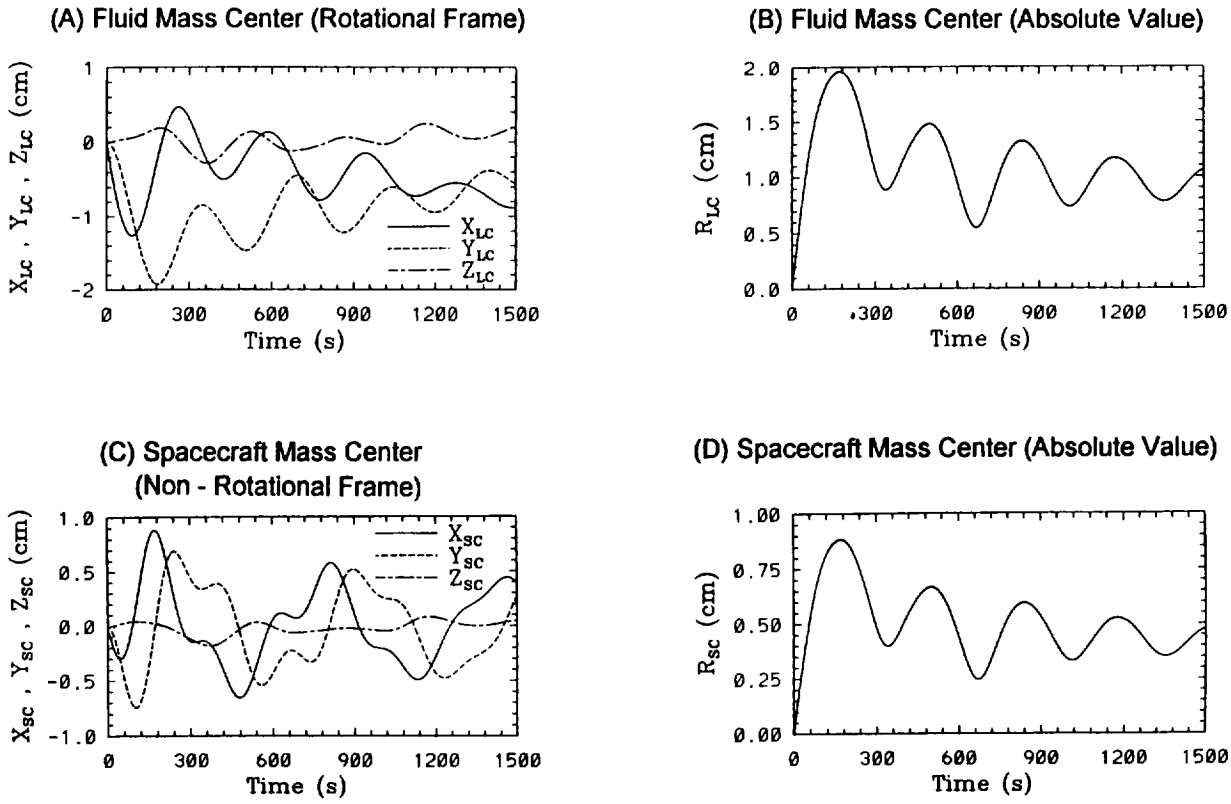

Figure 4 Time evolution of fluid and spacecraft mass centre fluctuations driven by coupling between lateral impulse and orbital dynamics. (A) Fluid mass centre in (x, y, z) components (rotational frame), (B) fluid mass centre (absolute value), (C) spacecraft mass centre in (X, Y, Z) components (non-rotational frame) and (D) spacecraft mass centre (absolute value)

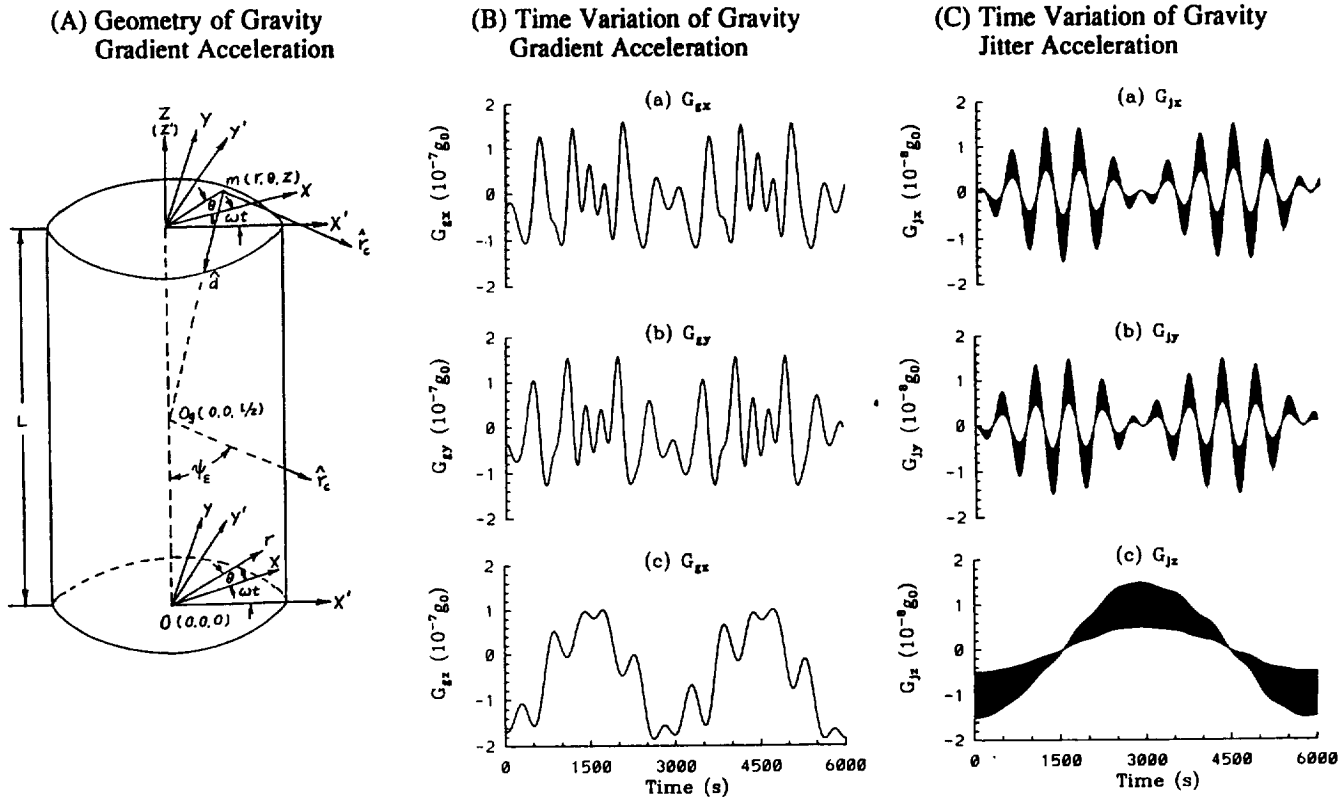

Figure 5 Time evolution of gravity gradient and g-jitter accelerations acting on the spacecraft during a full orbit period. (A) Geometry of gravity gradient acceleration, (B) time evolution of gravity gradient acceleration acting on fluid element located at (r, θ, z) = (40 cm, $\pi/4$, 10 cm) and (C) time evolution of g-jitter acceleration

where t is the time measured from the instant when the direction of the spacecraft's spinning axis is aligned with the radial direction from the spacecraft mass centre to the centre of the Earth. Some modification is required if the slosh and orbital dynamics are coupled and the results for the spacecraft orbit deviating from normal operation are considered.

Fluctuations in the residual gravity due to g-jitter acceleration are modelled by the following equation[18–20]:

$$g = g_B\left[1 + \frac{1}{2}\sin(2\pi ft)\right] \tag{16}$$

where g_B denotes the background gravity environment and f (Hz) stands for the frequency of the g-jitter.

In this study the following values have been considered[4] for the investigation of the oscillations of the liquid–vapour interface: g-jitter acceleration with a background gravity of 10^{-8} g_o due to spacecraft atmospheric drag, a rotating speed of 0.1 rev min^{-1} for normal GP-B spacecraft operation and 0.1, 1.0 and 10 Hz for the g-jitter frequencies. Components of the g-jitter acceleration in the non-inertial coordinate system are given by[18–20]

$$\begin{aligned}\hat{\mathbf{a}}_{gj} &= (a_{gj,r},\ a_{gj,\theta},\ a_{gj,z}) \\ &= [g\sin\psi_E\cos(\theta+\omega t),\ -g\sin\psi_E\sin(\theta+\omega t) \\ &\quad -g\cos\psi_E]\end{aligned} \tag{17}$$

The characteristics of the gravity gradient and jitter accelerations, shown in Equations (14) and (17), respectively, are quite different. The gravity gradient acceleration indicates the following two characteristics: (a) the acceleration acting on any fluid mass inside the container increases by two units of acceleration per unit of distance measured from the mass centre of the container (point O_g in *Figure 5A*) to the location of the fluid mass parallel to the radial axis from the mass centre of the container to the centre of the Earth (parallel to the unit vector $\hat{\mathbf{r}}_c$ shown in *Figure 5A*); and (b) the acceleration acting on the fluid mass decreases by one unit of acceleration per unit of the shortest distance measured from the location of the fluid mass to the radial axis along the vector from the mass centre of the container to the centre of the Earth[17–19]. As an example, *Figure 5B* shows the time variation of the gravity gradient accelerations for a full orbit period of 5856 s with container rotating speed of 0.1 rev min^{-1} for components along the (x, y, z) directions acting on the fluid mass located at (r, θ, z) = (40 cm, $\pi/4$, 10 cm). As the magnitude and direction of the gravity gradient acceleration acting on each fluid mass is strongly dependent on how far the location of the fluid mass deviates from the mass centre of the container measured along the axis parallel to the vector $\hat{\mathbf{r}}_c$, which varies with respect to time, it shows that the gravity gradient acceleration acting on the fluid mass is different for fluid masses at different locations in the container. The characteristics of symmetry are shown between the first and second half-orbit periods of the time evolution of gravity gradient acceleration if the orbit period is on an integral number of spacecraft spinning periods and the spacecraft is under normal operation[18–20]. Coupling of slosh and orbital dynamics resulted in *Figure 5B* and shows that the time evolution of the gravity gradient acceleration is asymmetric, whereas it is symmetric for the non-coupling case[18–20]. *Figure 5B* also shows that the magnitude of the gravity gradient accelerations is of the order of 10^{-7} g_o. Unlike gravity gradient accelerations of the fluid mass which have different magnitudes at different locations in the container, the g-jitter acceleration provides the same acceleration to the fluid mass at different locations in the container. *Figure 5C* shows the time variation of g-jitter accelerations for a full orbit period of 5856 s with a container rotating speed of 0.1 rev min^{-1} and a jitter frequency of 0.1 Hz for components along the (x, y, z)-directions acting on the fluid mass everywhere in the container. Again, symmetry is demonstrated between the first and second half-orbit periods of the time evolution of the g-jitter acceleration if the orbit interval is an integral multiple of the spacecraft spinning period and the spacecraft is under normal operation[18–20]. The coupling of slosh and orbital dynamics resulted in *Figure 5C* and shows that the time evolution of the g-jitter acceleration is asymmetric, whereas it is symmetric for the non-coupling case[18–20]. With the background gravity of 10^{-8} g_o for g-jitter acceleration considered in this study, the combined gravity gradient and g-jitter accelerations acting on the spacecraft correspond to the case of orbital accelerations dominated by gravity gradient forces (of the order of 10^{-7} g_o) acting on the fluid system of the spacecraft. In general, the magnitude range for g-jitter accelerations is 10^{-5} to 10^{-9} g_o.

Figure 6A shows the time-sequence evolution of the three-dimensional dynamical behaviour of interface oscillations driven by the combined gravity gradient and g-jitter accelerations and dominated by the gravity gradient force. The gravity gradient acceleration given by Equation (14) indicates that there are greater positive components of the acceleration longitudinal to the direction between the spacecraft mass centre and the centre of the Earth, and smaller negative components of acceleration transverse to this direction. As indicated in Equation (15), angle ψ_E varies with time. This phenomenon shows that the gravity gradient acceleration exerted on the fluid system of the spacecraft is equivalent to a combination of the time-dependent twisting force with turn-around direction and the torsional moment acting on the dewar when the spacecraft is orbiting around the Earth. *Figure 6A* shows that the deformation of the bubble is created by an asymmetric torsional moment with a twisting force.

The evolution of the capillary-effect-governed interface oscillations at various cross-sections driven by a gravity gradient-dominated acceleration is also examined. *Figure 6B* shows the time sequence of the capillary-effect-governed liquid–vapour interface profiles, driven by the same gravity gradient-dominated acceleration coupled with orbital dynamics as that shown in *Figure 6A*, in the vertical r–z plane at $\theta = 0°$ and 180°. This indicates that the doughnut-shaped bubble (helium vapour) configurations change from axial symmetric to asymmetric profiles in both planes as ψ_E varies from 0° to 360°.

The r–z cross-section of the doughnut profiles shows oscillations of two bubbles in *Figure 6B*. Here, the one-up one-down and one-down one-up oscillations indicate a very important characteristic of the gravity gradient-dominated acceleration which produces a combination of a time-dependent equivalent torsional moment and a twisting force acting on the fluid system of the spacecraft when it is orbiting around the Earth.

In addition to the 0.1 Hz low-frequency gravity gradient-dominated acceleration, 1.0 Hz medium-frequency and

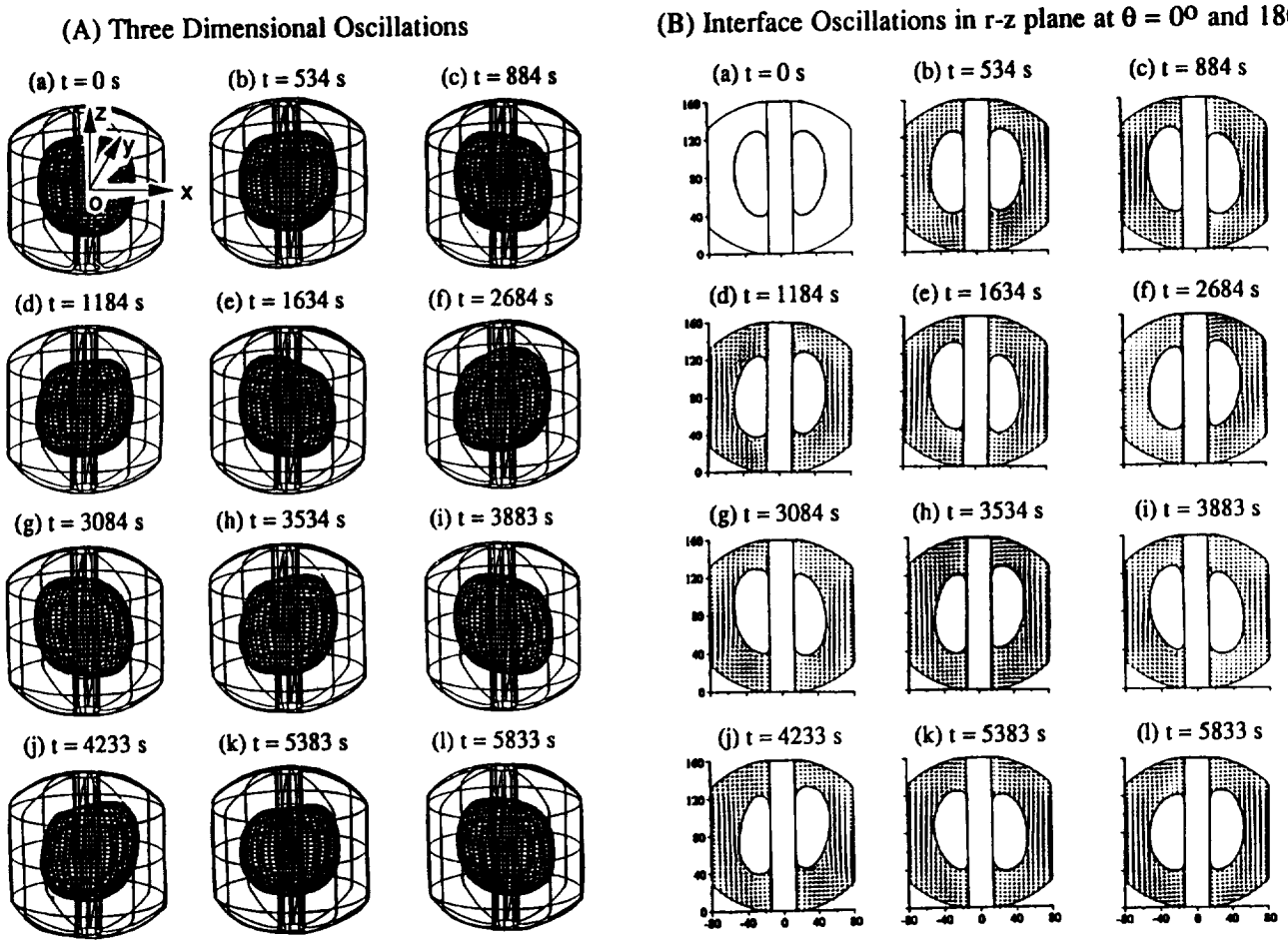

Figure 6 Three-dimensional bubble deformations in response to coupling between gravity gradient-dominated accelerations and orbital dynamics

10 Hz high-frequency g-jitter acceleration-driven liquid–vapour interface oscillations have also been investigated. Characteristics of these three ranges of g-jitter frequencies were well documented in earlier studies[4,5]. Results show that lower-frequency g-jitter accelerations contribute more in the driving of asymmetric profiles of the interface than the higher-frequency g-jitter accelerations. These results are in agreement with the earlier studies[4,5].

Figure 7A shows sloshing due to the time evolution of fluid mass centre fluctuations (in the rotational frame) driven by gravity gradient-dominated acceleration coupling with orbital dynamics. The values of the maximum and minimum locations of the fluid mass centre fluctuations are Max (x_{LC}, y_{LC}, z_{LC}) = (0.74, 0.72, 1.35) cm and Min (x_{LC}, y_{LC}, z_{LC}) = (−0.73, −0.67, −0.01) cm, respectively, while the fluctuating values of the maximum fluid mass centre disturbances are Max (Δx_{LC}, Δy_{LC}, Δz_{LC}) = (1.4, 1.4, 1.3) cm. This shows that $\Delta x_{LC} \sim \Delta y_{LC} > \Delta z_{LC}$. Results of fluid mass centre fluctuations driven by gravity gradient-dominated acceleration coupling with orbital dynamics can be summarized as follows: (a) fluid mass centre oscillations along the x- and y-directions basically follow the trends of the time-dependent evolution of gravity gradient accelerations along the x- and y-axes in a tidal mode manner[19–23] of coupling with orbital dynamics, as shown in *Figures 5B-a* and *5B-b*; (b) there are fluid mass centre fluctuations with a smaller amplitude along the z-axis in response to the trend of the time-dependent evolution of the gravity gradient acceleration along the z-axis in a similar manner; (c) coupling between slosh and orbital dynamics also results in an asymmetric tendency of a tidal mode nature[19–23] of the fluid mass centre fluctuations while the spacecraft is orbiting around the Earth; (d) there is a time lag of 150 s between the moment when the gravity gradient-dominated accelerations act on the spacecraft and the time when fluid mass centre fluctuations reach their maximum – in other words, the maximum of the fluid mass centre fluctuations was not reached instantly and did not change its direction at the moment the gravity gradient force changed direction; (e) *Figure 7B* shows the time history of the liquid mass centre fluctuations. Large-amplitude fluctuations correspond to the directional change of the gravity gradient with respect to the azimuth angle variation, while the small ripples imposed on the oscillations are contributed by the slosh dynamics.

Spacecraft system mass centre fluctuations (in a non-rotational frame) in response to the coupling between slosh dynamics driven by a gravity gradient-dominated force and orbital dynamics deviating from normal operation have been studied, and are illustrated in *Figure 7C*. The values of the maximum and minimum locations of spacecraft mass centre fluctuations are Max (X_{sc}, Y_{sc}, Z_{sc}) = (0.35, 0.29, 0.60) cm and Min (X_{sc}, Y_{sc}, Z_{sc}) = (−0.34, −0.32, −0.07) cm, respectively, while the fluctuating values of the maximum spacecraft mass centre disturbances are Max (ΔX_{sc}, ΔY_{sc}, ΔZ_{sc}) = (0.69, 0.61, 0.67) cm. This shows that $\Delta X_{sc} \sim \Delta Y_{sc} \sim \Delta Z_{sc}$ in a non-rotational frame. The results are very similar to those concluded from the fluid mass

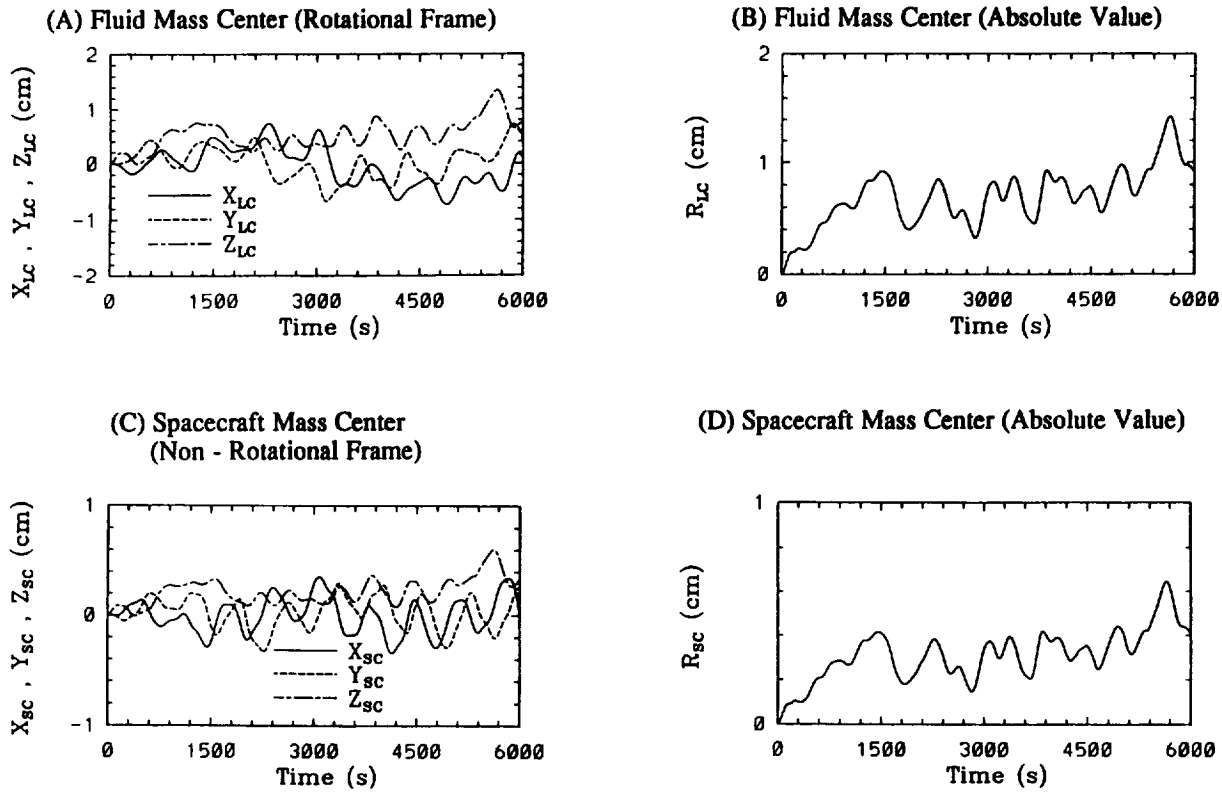

Figure 7 Time evolution of fluid and spacecraft mass centre fluctuations driven by gravity gradient-dominated acceleration and orbital dynamics. (A) Fluid mass centre in (*x, y, z*) components (rotational frame), (B) fluid mass centre (absolute value), (C) spacecraft mass centre in (*X, Y, Z*) components (non-rotational frame) and (D) spacecraft mass centre (absolute value)

centre fluctuations obtained in the previous section, except that (a) the former case is in a non-rotational frame and the latter case is in rotational frame and (b) the former case has smaller fluctuations due to the effect of averaging between the dry mass of the spacecraft and the fluid mass fluctuations. *Figure 7D* shows the time-dependent variation in the absolute value of the spacecraft system mass centre fluctuations. Comparison between *Figures 7B* and *7D* shows that the spacecraft mass centre fluctuations are mainly dominated by the fluid system mass centre fluctuations. Failure to consider the effect of slosh dynamics acting on the spacecraft may lead to the wrong results for the case of a gravity gradient-dominated acceleration acting on the orbiting spacecraft.

Coupling between slosh dynamics driven by combined gravity gradient and g*-jitter accelerations dominated by* g*-jitter forces and spacecraft dynamics*

In this case, combined gravity gradient and *g*-jitter with an amplitude of 10^{-6} g_o for *g* shown in Equation (17) is considered. The gravity gradient acceleration in this case is shown in *Figure 5B*, while the *g*-jitter acceleration with background amplitude of 10^{-8} g_o, shown in *Figure 5C*, is replaced by 10^{-6} g_o for the present case. Then the combined gravity gradient (of the order of $10^{-7}g_o$) and *g*-jitter accelerations acting on the spacecraft correspond to the case of orbital accelerations dominated by *g*-jitter forces acting on the fluid system of the spacecraft. As indicated earlier, *g*-jitter accelerations are in the range 10^{-5} to 10^{-9} g_o.

Figure 8A shows the time sequence evolution of the three-dimensional dynamic behaviour of interface oscillations driven by combined gravity gradient and *g*-jitter accelerations dominated by a *g*-jitter force of 0.1 Hz low-jitter frequency. The *g*-jitter acceleration, shown in Equations (16) and (17) and illustrated in *Figure 5C*, indicates that there is a sinusoidal oscillation longitudinal to the direction from the spacecraft mass centre to the centre of the Earth (parallel to unit vector $\hat{\mathbf{r}}_c$ shown in *Figure 5A*). As indicated in Equation (15), the azimuth angle ψ_E varies with time. These phenomena show that the *g*-jitter acceleration exerted on the fluid system of the spacecraft is equivalent to the oscillatory forces that push the bubble in the combined directions of down–up (see *z*-component of *g*-jitter acceleration shown in *Figure 5C*) and left–right (see *x*- and *y*-components of *g*-jitter accelerations shown in *Figure 5C* as the bubble rotates with respect to the spacecraft spinning axis. Time variations in the *x*- and *y*-components of the *g*-jitter accelerations, shown in *Figure 5C*, characterize the left–right oscillations of bubbles shown in *Figures 8A* and *8B*. *Figure 8B* shows the time sequence of the liquid–vapour interface profiles in the vertical *r*–*z* plane at $\theta = 0°$ and 180°. Among the various frequencies of the *g*-jitter-dominated accelerations considered, it is shown that lower-frequency *g*-jitter accelerations contribute more to the driving of asymmetric profiles of the interface than higher frequency *g*-jitter accelerations[32,33].

Figure 9A shows sloshing due to the time evolution of the fluid mass centre fluctuations (in a rotational frame) driven by *g*-jitter-dominated acceleration coupling with orbital dynamics. The values of the maximum and minimum locations of the fluid mass centre fluctuations are Max (x_{LC}, y_{LC}, z_{LC}) = (1.19, 1.21, 3.53) cm and Min (x_{LC}, y_{LC}, z_{LC}) = (−1.20, −1.03, −1.84) cm, respectively, while the fluctuating values of the maximum fluid mass centre disturbances are Max (Δx_{LC}, Δy_{LC}, Δz_{LC}) = (2.38, 2.24, 5.37) cm. This shows that $z_{LC} > x_{LC} > y_{LC}$. Results of fluid mass

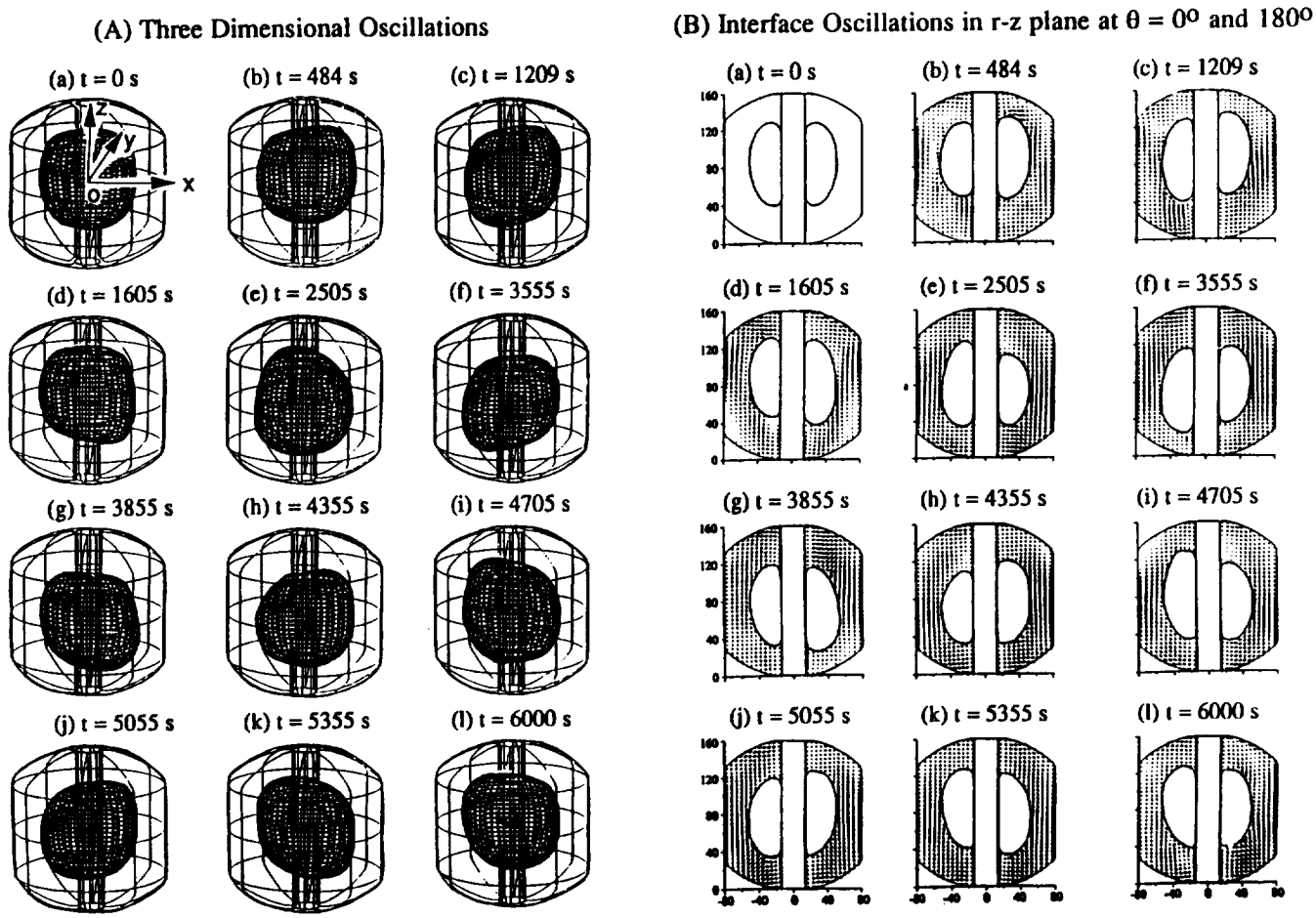

Figure 8 Three-dimensional bubble deformations in response to coupling between *g*-jitter-dominated accelerations and orbital dynamics

centre fluctuations driven by *g*-jitter-dominated acceleration coupling with orbital dynamics can be summarized as follows: (a) fluid mass centre oscillations along the *x*- and *y*-directions basically follow the trends of the time-dependent evolution of *g*-jitter accelerations in the *x*- and *y*-axis coupling with orbital dynamics shown in *Figures 5C-a* and *5C-b*; (b) fluid mass centre fluctuations have greater amplitudes along the *z*-axis in response to the trend of the time-dependent evolution of a *g*-jitter acceleration along the *z*-axis in which one half of the orbit period is in the positive and the other in the negative direction – this result is exactly reflected by the fluid mass centre fluctuations along the *z*-axis shown in *Figure 9A* with small ripples imposed by slosh dynamics; (c) coupling between slosh and orbital dynamics also results in the asymmetric nature of the fluid mass centre fluctuations while the spacecraft is orbiting around the Earth; (d) there is a time lag of 150 s between the moment when the *g*-jitter-dominated accelerations act on the spacecraft and the time when maximum fluid mass centre fluctuations are reached – in other words, the fluid mass centre fluctuations react rather slowly and do not instantly change direction when the *g*-jitter direction changes; (e) *Figure 9B* shows the time-dependent variation of the absolute value of fluid mass centre fluctuations resulting from coupling between the slosh and orbital dynamics. It shows time-dependent fluctuations with large amplitudes corresponding to directional changes in *g*-jitter with respect to azimuth angle, while the small ripple imposed on the oscillations is contributed by the slosh dynamics.

Spacecraft system mass centre fluctuations (in a non-rotational frame) in response to the coupling between slosh dynamics driven by a *g*-jitter-dominated force and orbital dynamics deviating from normal operation have been studied, and are illustrated in *Figure 9C*. The values of the maximum and minimum locations of the spacecraft mass centre fluctuations are Max (X_{sc}, Y_{sc}, Z_{sc}) = (0.29, 0.43, 1.6) cm and Min (X_{sc}, Y_{sc}, Z_{sc}) = (−0.21, −0.21, −0.83) cm, respectively, while the fluctuating values of the maximum spacecraft mass centre disturbances are Max (ΔX_{sc}, ΔY_{sc}, ΔZ_{sc}) = (0.5, 0.7, 2.5) cm. This shows that $\Delta Z_{sc} > \Delta Y_{sc} > \Delta X_{sc}$ in a non-rotational frame. Results of spacecraft mass centre fluctuations driven by coupling of a *g*-jitter-dominated force and orbital dynamics are very similar to those driven by gravity-gradient dominated force and spacecraft dynamics. Failure to consider the effect of slosh dynamics acting on the spacecraft may lead to the wrong results for the case of a *g*-jitter-dominated acceleration acting on the orbiting spacecraft.

Characteristics of various orbital accelerations considered in this study, in addition to the results obtained from the previous section for He II slosh dynamics driven by various accelerations coupled with orbital dynamics, are summarized and illustrated in *Table 1*.

Conclusions

The coupling of motions in a spinning spacecraft dewar activated by (a) lateral impulse, (b) gravity gradient-domi-

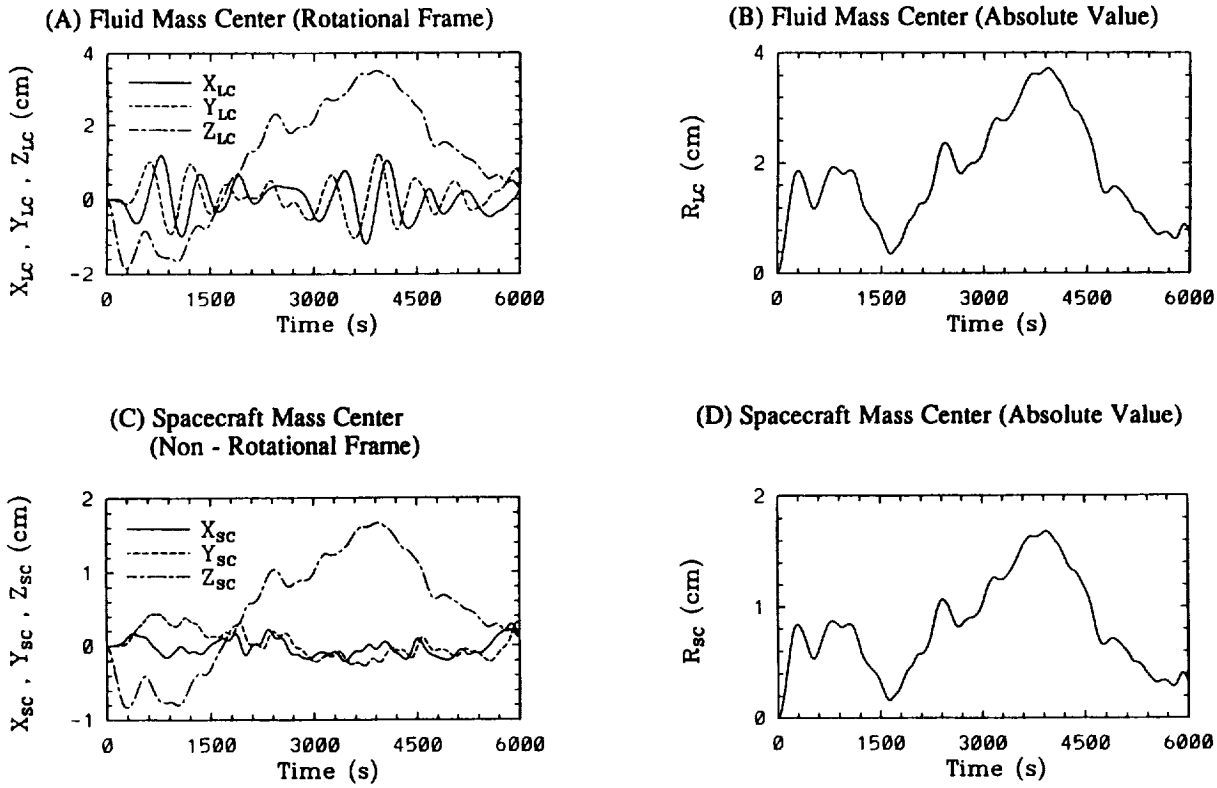

Figure 9 Time evolution of fluid and spacecraft mass centre fluctuations driven by *g*-jitter-dominated accelerations and orbital dynamics. (A) Fluid mass centre in (*x, y, z*) components (rotational frame), (B) fluid mass centre (absolute value), (C) spacecraft mass centre in (*X, Y, Z*) components (non-rotational frame) and (D) spacecraft mass centre (absolute value)

nated and (c) *g*-jitter-dominated accelerations with spacecraft orbital dynamics has been investigated. It is shown that coupling between He II slosh dynamics and orbital dynamics can cause large-amplitude fluctuations to act on a spacecraft, resulting in deviations from normal operation.

For the purpose of this study, the slosh dynamics are based on a rotational frame, while the orbital dynamics are associated with a non-rotational frame. Computation of He II slosh dynamics and the fluctuations of the spacecraft mass centre, driven by the three types of force, indicate that the major contribution of the orbital dynamics is driven by those forces coupling with slosh dynamics. Among these three environmental and impulsive forces acting on the spacecraft, both the gravity-gradient and *g*-jitter forces are in the form of a continuous spectrum while the impulse is in the form of a spotty δ-function. All these forces are capable of exciting slosh dynamics coupling with orbital dynamics. In fact, failure to consider the effect of slosh dynamics acting on the spacecraft may lead to the wrong results. The asymmetric orientation of the helium II liquid sloshing in the tank driven by the three forces considered may also create control and pointing problems causing deviation from normal spacecraft operation[5,19].

Acknowledgement

The authors appreciate the support received from the National Aeronautics and Space Administration through the NASA Grant NAG8-938 and NASA Contract NAS8-39609/Delivery Order No. 103.

References

1 **Avduyevsky, V.S.** (Ed) *Scientific Foundations of Space Manufacturing* MIR, Moscow, USSR (1984)
2 **Forward, R.L.** *Physical Review, Series (A)* (1982) **26** 735
3 **Misner, C.W., Thorne, K.S. and Wheeler, J.A.** *Gravitation* W.H. Freeman and Co., San Francisco, CA (1973)
4 **Kamotani, Y., Prasad, A. and Ostrach, S.** *AIAA J* (1981) **19** 511
5 **Hung, R.J., Lee, C.C. and Leslie, F.W.** *J Guidance, Control and Dynamics* (1992) **15** 817
6 **Hung, R.J., Lee, C.C. and Leslie, F.W.** *J Fluids and Struct* (1992) **6** 493
7 **Hung, R.J., Tsao, Y.D., Hong, B.B. and Leslie, F.W.** *J Spacecraft and Rockets* (1989) **26** 167
8 **Leslie, F.W.** *J Fluid Mech* (1985) **161** 269
9 **Mason, P., Collins, D., Petrac, D., Yang, L., Edeskuty, F., Schuch, A. and Williamson, K.** *Proc ICEC7* IPC Science and Technology Press, Guildford, UK (1978)
10 **Donnelly, R.J.** *Scientific American* (Nov 1988) 100
11 **Van Sciver, S.W.** *Helium Cryogenics* Plenum Press, New York (1986)
12 **Donnelly, R.J.** *Quantized Vortices in Helium II* Cambridge University Press, Cambridge (1991)
13 **Wilks, J. and Betts, D.S.** *An Introduction to Liquid Helium* Clarendon Press, Oxford, UK (1987)
14 **Hung, R.J., Pan, H.L. and Long, T.Y.** *Cryogenics* (1994) **34** 641
15 **Hung, R.J. and Long, T.Y.** *Cryogenics* (1995) **35** 589
16 **Wilks, J.** *The Properties of Liquid and Solid Helium* Clarendon Press, Oxford, UK (1967)
17 **Hoare, F.E., Jackson, L.C. and Kurti, N.** *Experimental Cryogenics: Liquid Helium II* Butterworths, London, UK (1961)
18 **Hung, R.J. and Long, Y.T.** *Trans Jpn Soc for Aeronautical and Space Sci* (1995) **37** 291
19 **Hung, R.J. and Pan, H.L.** *J Guidance, Control, and Dynamics* (1995) **18** 1190
20 **Hung, R.J. and Pan, H.L.** *Trans Jpn Soc for Aeronautical and Space Sci* (1993) **36** 153
21 **Hung, R.J. and Pan, H.L.** *Fluid Dynamics Res* (1994) **34** 29
22 **Hung, R.J. and Pan, H.L.** *Appl Math Modelling* (1995) **19** 483
23 **Hung, R.J., Pan, H.L. and Leslie, F.W.** *J Flight Sci Space Res* (1994) **18** 195
24 **Hung, R.J. and Pan, H.L.** *Acta Mech Sinica* (1993) **9** 298
25 **Hung, R.J. and Leslie, F.W.** *J Spacecraft and Rockets* (1988) **25** 70
26 **Harlow, F.H. and Welch, F.E.** *Phys Fluids* (1965) **8** 2182
27 **Rubin, S.G. and Lin, T.C.** *J Computational Phys* (1972) **9** 339

28 **Salvadori, M.G. and Baron, M.L.** *Numerical Methods in Engineering* Prentice-Hall, Inc., Englewood Cliffs, NJ (1961)
29 **Hageman, L.A. and Young, D.M.** *Applied Iterative Methods* Academic Press, New York (1981)
30 **Young, D.** *Trans Am Math Soc* (1954) **76** 92
31 **Patanker, S.V.** *Numerical Heat Transfer and Fluid Flow* Hemisphere/McGraw-Hill, New York, NY (1980)
32 **Hung, R.J., Lee, C.C. and Leslie, F.W.** *Trans Jpn Soc for Aeronautical and Space Sci* (1993) **35** 187
33 **Hung, R.J. and Lee, C.C.** *J Spacecraft and Rockets* (1994) **31** 1107
34 **Greenwood, D.T.** *Principles of Dynamics* Prentice-Hall, Englewood Cliffs, NJ (1965)